RESEARCH ARTICLE

Expression profiles of long noncoding RNAs in retinopathy of prematurity

Yue Wang, Xue Wang, Yuan Ma, Yue-Xia Wang, Yu Di*
Department of Ophthalmology, Shengjing Hospital of China Medical University, Shenyang, Liaoning Province, China

Funding: *The work was supported by the National Natural Science Foundation of China, No. 81600747 (to YD) and Startup Foundation for Doctors of Liaoning Province, China, No. 201501020 (to YD).*

Graphical Abstract

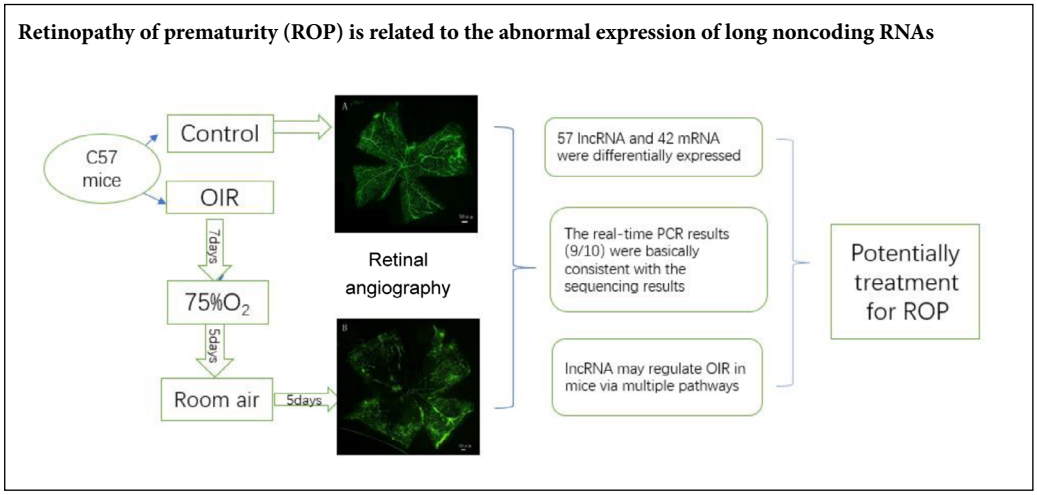

***Correspondence to:**
Yu Di, MD, diyu81@126.com.

orcid:
0000-0001-6664-2952
(Yu Di)

doi: *10.4103/1673-5374.280328*

Received: *November 17, 2019*
Peer review started: *November 20, 2019*
Accepted: *January 16, 2020*
Published online: *April 3, 2020*

Abstract

Long noncoding RNA (lncRNA) regulates the proliferation and migration of human retinal endothelial cells, as well as retinal neovascularization in diabetic retinopathy. Based on similarities between the pathogenesis of retinopathy of prematurity (ROP) and diabetic retinopathy, lncRNA may also play a role in ROP. Seven-day-old mice were administered 75 ± 2% oxygen for 5 days and normoxic air for another 5 days to establish a ROP model. Expression of lncRNA and mRNA in the retinal tissue of mice was detected by high-throughput sequencing technology, and biological functions of the resulted differentially expressed RNAs were evaluated by Gene Ontology and Kyoto Encyclopedia of Genes and Genomes analyses. The results showed that compared with the control group, 57 lncRNAs were differentially expressed, including 43 upregulated and 14 downregulated, in the retinal tissue of ROP mice. Compared with control mice, 42 mRNAs were differentially expressed in the retinal tissue of ROP mice, including 24 upregulated and 18 downregulated mRNAs. Differentially expressed genes were involved in ocular development and related metabolic pathways. The differentially expressed lncRNAs may regulate ROP in mice via microRNAs and multiple signaling pathways. Our results revealed that these differentially expressed lncRNAs may be therapeutic targets for ROP treatment. This study was approved by the Medical Ethics Committee of Shengjing Hospital of China Medical University on February 25, 2016 (approval No. 2016PS074K).

Key Words: *bioinformatics; gene therapy; long noncoding RNA; microglial; neurovascular disease; optic neuropathy; retinal development; retinal neovascularization; retinopathy of prematurity; signaling pathways*

Chinese Library Classification No. *R446; R741; Q522+.6*

Introduction

Retinopathy of prematurity (ROP) is a retinal vascular proliferation disease with neuronal degeneration (Mehdi et al., 2014; Tsang et al., 2019). ROP occurs in premature infants with retinal vascular proliferation, especially those with very low birth weights (Gonski et al., 2019). The main clinical manifestations of ROP are retinal ischemia, retinal neovascularization (RNV), and even retinal detachment, which can lead to childhood blindness (Aranda et al., 2019). Even with immediate and effective treatment, ROP may damage retinal nerves and blood vessels (Wang et al., 2005; Le, 2017); previous studies have shown this to be associated with a high density of microglia and retinal astrocytes in the central vascular area (Bucher et al., 2013; Xu et al., 2018).

Long noncoding RNAs (lncRNAs) are involved in multiple diseases, including RNV. Increasing evidence indicates that lncRNAs are related to the development of tumors and neovascular diseases (Xu et al., 2014; Chen et al., 2017a; Long et al., 2018). In addition, lncRNAs can regulate microglial polarization and inflammation (Wang et al., 2019; Yang et al., 2019; Zhang et al., 2019c). A few studies have shown that lncRNAs exhibit tissue-specific expression in the eye (Young

et al., 2005; Qiu et al., 2016). lncRNA has the function of competing with endogenous RNA or microRNA to regulate the proliferation and migration of human retinal endothelial cells, as well as RNV in diabetic retinopathy (Zhu et al., 2017; Fan et al., 2019). Based on its similarities with the pathogenesis of diabetic retinopathy, RNV in ROP may be explained by similar molecular mechanisms. As such, this study aimed to decipher the role of differential expressed lncRNA in oxygen-induced retinopathy (OIR) mice and explore how abnormal lncRNA expression affects the hypoxic process of ROP. We hope that our research on differentially expressed lncRNA can provide a theoretical basis for the identification of new clinical treatments for ROP.

Materials and Methods

Animals and OIR model

Seven-day-old C57BL/6J mice (n = 100; specific pathogen-free level) were purchased from Shenyang Changsheng Biological Technology Co, Ltd. [Shenyang, China; license No. SCXK(Liao)2015-0001]. Mice were bred at the specific pathogen-free Laboratory Animal Center of Shengjing Hospital (Benxi, China) at 23 ± 2°C with 12-hour light-dark cycles. The Medical Ethics Committee of Shengjing Hospital of China Medical University approved the animal experiments on February 25, 2016 (approval No. 2016PS074K).

Animals were randomly divided into two groups with 50 mice in each group. Mice in the control group were kept in normoxic air with their mothers until the age of 17 days. In the experimental group, OIR was induced according to Smith's method (Smith et al., 1994). Briefly, 7-day-old mice in the OIR group and their mother were placed for 5 days in a hyperoxia chamber provided by the Laboratory Animal Center of Shengjing Hospital, which was composed of glass feeding box, oxygen detector (8F-3AW; Yuwell, Suzhou, China), and oxygen generator (OX-100A; Aipuins, Hangzhou, China) (75 ± 2%). Subsequently, these mice were maintained in normoxic air for another 5 days with their mothers (Smith et al., 1994; Heiduschka et al., 2019). Mice in both groups were sacrificed to collect retinas for total RNA extraction and pathology after deep anesthesia with ketamine at postnatal day 17 (Park et al., 2009).

Retina isolation and fluorescein isothiocyanate-dextran angiography

Seventeen-day-old mice were anesthetized with ketamine, and 500 μL of fluorescein isothiocyanate-dextran (2×10^3 kDa; 50 mg/mL; Sigma-Aldrich, St. Louis, MO, USA) was injected into the left ventricle; 2 minutes later, mice were sacrificed by cervical dislocation. Next, the eyes were enucleated and fixed with 4% paraformaldehyde for 2 hours at 4°C. After removing the cornea, lens, and vitreous, retinas were peeled from the eyeball and cut into four quadrants with an ophthalmic scalpel under a stereomicroscope (SMZ18; Nikon, Tokyo, Japan). Images were captured under a fluorescence microscope (Eclipse NI, Nikon) before applying SlowFade anti-fade reagent (Sigma-Aldrich) to retinas (Banin et al., 2006; Geng et al., 2018). The lasso tool of Adobe Photoshop CS6 (Adobe, San Francisco, CA, USA) was used to manually select areas of non-perfusion and neovascular retinal tufts. ImageJ 1.37C (National Institutes of Health, Bethesda, MD, USA) was used to automatically calculate the percentage areas selected by Photoshop CS6 (Zhang et al., 2000; Shi et al., 2013). All manual work was completed by three reviewers.

Hematoxylin-eosin staining

Ten randomly selected mice from each group were fixed for 24 hours. The eyeball was cut along the sagittal plane parallel to the optic nerve and embedded in paraffin. Next, the eyeball was cooled to room temperature to prepare a 3.5-μm-thick continuous slice, and 10 pieces from each eyeball were selected for hema-toxylin-eosin staining. Images were captured under a fluorescence microscope, and the average number of all neovascular nuclei present in the vitreous side were counted for each section by three independent reviewers in a double-blind manner (Zhang et al., 2017).

RNA extraction and preparation

Total RNA from each retinal tissue sample was extracted using TRIzol reagent (Takara, Kusatsu, Japan) and quantified by Nanodrop ND-2000 (Thermo Scientific, Waltham, MA, USA). RNA integrity was detected by an Agilent Bioanalyzer 2100 (Agilent Technologies, Santa Clara, CA, USA). We selected samples with optical density$_{260/280}$ = 1.8–2.0 for subsequent experimental studies. Chip processing was subsequently performed according to Agilent's standards, including sample labeling, microarray hybridization, and washing.

Array analysis

Analysis of lncRNA and mRNA array data was achieved by Feature extraction (version 10.7.1.1; Agilent Technologies). Normalization of raw data by quantile and quality control was performed using GeneSpring (version 13.1; Agilent Technologies). The threshold set for screening of differentially expressed genes was fold change ≥ 2 and $P < 0.05$. Gene Ontology (GO) and Kyoto Encyclopedia of Genes and Genomes (KEGG) analyses were used to determine the effect of differentially expressed genes. Numbers and significance of differentially expressed genes included in each GO entry were counted (http://geneontology.org/). The KEGG database was used to analyze differentially expressed genes and calculate the significance of differences in gene enrichment for each pathway entry (http://www.genome.jp/kegg/).

Hierarchical clustering was used to verify differences in gene expression patterns between samples and calculate the distance between different samples to generate a distance matrix. Finally, String was used to constructing a protein interaction network using vascular endothelial growth factor (VEGF) and other dif-ferentially expressed mRNAs (Qu et al., 2017; Liu et al., 2018).

Quantitative real-time PCR

Total RNA extraction and quality control were performed as described above. Ten lncRNAs in retinal tissues were

measured by quantitative real-time PCR (qRT-PCR) using SYBR® Green assays (Takara) with the primers listed in **Table 1** (Sangon Biotech Co., Ltd., Shanghai, China). β-Actin was applied as an internal control. For quantitative analysis of differential expression, data were processed by the $2^{-\Delta\Delta Ct}$ method, and expression of each lncRNA is expressed as the relative fold change to β-actin.

Statistical analysis

All statistical data are expressed as the mean ± standard error of mean (SEM). Differences were analyzed by Mann-Whitney *U* test using SPSS 17.0 (Release 17.0; SPSS Inc., Chicago, IL, USA). *P*-values < 0.05 were considered statistically significant.

Results

Retinal neovascularization in OIR mice

Retinal vascular structures were examined by fluorescein isothiocyanate-dextran angiography. Expectedly, the retinal vasculature of control group mice was intact, with the main blood vessels and vessel branches arranged regularly (**Figure 1A** and **C**). In the OIR group, the retina of mice showed severe areas without perfusion, as well as neovascularization and distorted blood vessels with irregular dilation (**Figure 1B** and **D**). Percentage areas of non-perfusion and neovascularization in the OIR group were higher compared with the control group ($Z = -2.882$, $P = 0.004$; $Z = -2.739$, $P = 0.006$; **Figure 1E** and **F**).

Neovascular nuclei of the retina in OIR mice

We quantified retinal neovascular nuclei from 10 non-continuous paraffin sections of the retina, primarily by calculating the number of neovascular nuclei that broke through the inner limiting membrane of the retina. In the control group, retinal neovascular nuclei were rarely observed, with an average number of 2.70 ± 0.58 nuclei per cross-section (**Figure 2A**). In the OIR group, an average of 20.70 ± 2.53 nuclei was observed for each retina cross-section (**Figure 2B**), which is significantly larger than observed in the control group ($Z = -3.686$, $P < 0.01$; **Figure 2C**).

Differentially expressed lncRNAs and mRNAs in the retinal tissue of OIR mice

In total, 62,028 distinct lncRNAs and 33,419 mRNAs were detected in the retinal tissue of experimental mice using high-throughput sequencing technology. Compared with the control group, 57 lncRNAs and 42 mRNAs were differentially expressed, 43 lncRNAs and 24 mRNAs were significantly upregulated, and 14 lncRNAs and 18 mRNAs were significantly downregulated in the OIR group (fold change ≥ 2, $P < 0.05$). A volcano plot of differentially expressed genes reflects their trends (**Figure 3A**), while scatter plots indicate better data normalization (**Figure 3B**). Most genes were concentrated on chromosomes 4, 7, 11, and 14 (**Figure 3C**). Cluster analysis showed that lncRNA were differentially expressed in both control mice and the OIR group (**Figure 3D**).

We validated the top five upregulated and top five downregulated genes in the two sets of retina samples by qRT-PCR; information about these genes is listed in **Table 1**. For nine of the ten genes, qRT-PCR results were consistent with the sequencing results, not including AC142098.2 (**Figure 3E**).

Table 1 Primers used for quantitative real-time polymerase chain reaction

Gene	Type	Fold change	Chromosome	Primer (5′–3′)
LOC102637887	lncRNA	3.7505	7	F: CCC TGC TCC CTG TCG TGG TAG R: GCC TGT GTC TCG GTG ACT GTT C
LOC102638971	lncRNA	2.1859	5	F: GGC AGG CAC CAA AGC AGA GAC R: AGG AAC CGT GGA AGC CAG AGG
1700091H14Rik	lncRNA	2.4564	6	F: TGA GCA GGA GAA GAG ACA CGA GAG R: AGG AAC CGT GGA AGC CAG AGG
9030404E10Rik	lncRNA	4.8791	9	F: CTC GCT CAC CTC TGG ACT CCT G R: GCG TCA ATC CTC ACA GCC TTG G
1700026D11Rik	lncRNA	4.9759	X	F: CCT CGT CTT CCT GTT CAT CTG TGG R: GTG TCC TGC TAG GCA TAG TCC ATG
AC142098.2	lncRNA	4.6893	14	F: AGG AAG ACA GGA GCG GCA GAC R: TCC TCC ACC GAA CCG CAC TC
ENSMUST00000051401	mRNA	8.6844	5	F: TTA TGG TCA TCA GCA TCA TCG T R: TGA TCA TGA TCT TGG CCT TGA C
ENSMUST00000047095	mRNA	4.627	14	F: TTC TCA ATG GGC AAA AAG TCT G R: CTT GAA TGG CCT TGT TCT CTT C
ENSMUST00000005810	mRNA	29.8212	10	F: TGG CTT TCA TGT CAT TAA CGT G R: GAT ATT GTG ACT GTG GCA TCA C
ENSMUSG00000019961	mRNA	24.3167	6	F: TGA ATC GAG ATC CTC TAC TCC T R: GCT GTA TCT GTC AGA GTC GTT A
β-Actin	Maker	–	–	F: GTG CTA TGT TGC TCT AGA CTT CG R: ATG CCA CAG GAT TCC ATA CC

F: Forward; lncRNA: Long noncoding RNA; R: reverse.

Gene function analysis of differentially expressed genes in the retinal tissue of OIR mice

To analyze gene functions, GO, KEGG, and pathway cluster analyses were performed. Differentially ex-pressed genes were involved in more than 20 pathways and many processes, mainly associated with com-plement activation, the lectin pathway, nuclear factor-κB (NF-κB)-inducing kinase/NF-κB signaling pathway, G protein-coupled receptor signaling pathway, and canonical Wnt signaling pathway, suggesting that lncRNAs regulate oxygen-induced retinal neovascularization by various signaling pathways (**Figure 4**).

Protein interaction network of RNV

Based on differentially expressed mRNAs, VEGF mRNA was selected as the main mRNA in the protein interaction network because most of the remaining differentially expressed mRNAs were associated with VEGF; thus, differentially expressed mRNAs may be related to RNV (**Figure 5**).

Discussion

Normal development of the retina provides nutrition for photoreceptor cells and has regenerative and repair functions (Ishikawa et al., 2015; Morken et al., 2019). ROP is a serious neurovascular disease. However, currently used drugs, which are administered be intravitreal injection, only control neovascularization and have no effect on protecting nerve function (Kang et al., 2019; Tsang et al., 2019). Previous studies have shown that nerve growth factor, progenitor cells, and bone marrow mesenchymal stem cells can contribute to the recovery of OIR in mice (Li Calzi et al., 2019; Ma et al., 2019; Troullinaki et al., 2019). Moreover, progenitor cells in combination with other treatments can normalize retinal vascular development (Li Calzi et al., 2019), and are associated with lncRNAs (Yao et al., 2019; You and You, 2019). An increasing number of studies have shown that lncRNAs exert essential functions in cancer cells, particularly during proliferation, differentiation, and malignant transformation (Shen et al., 2016; Zhang et al., 2019a). Furthermore, lncRNAs are involved in choroidal neovascularization, proliferative vitreoretinopathy, and diabetic retinopathy (Yu et al., 2019; Zhang et al., 2019b). In addition, they contribute to retinal microangiopathy by regulating cell proliferation, apoptosis, inflammatory responses, and VEGF expression (Nieminen et al., 2018; Wei et al., 2019). Thus, they may regulate target gene expression in ROP; however, the specific molecular mecha-nisms underlying retinal vasculogenesis and angiogenesis in ROP have yet to be determined. In this study, the OIR mouse model and high-throughput sequencing were used to detect lncRNAs involved in the path-ogenesis of ROP.

GO and KEGG analyses were used to gain insight into the functions of lncRNAs in OIR. Abnormally ex-pressed genes were widely distributed in retinal tissues and found to be components of signaling pathways related to retinal development and function, such as NF-κB, G protein-coupled receptor, and canonical Wnt signaling pathways. Previous studies suggested that lncRNAs competitively block the binding of mRNAs to microRNAs to exert anti-oxidative and anti-inflammatory roles in retinal endothelial cells via the NF-κB sig-naling pathway, thereby inhibiting angiogenesis (Hui and Yin, 2018; Ruan et al., 2018; Chen et al., 2019). We speculate that the mechanisms by which lncRNAs regulate retinopathy in OIR mice are similar to those involved in diabetic retinopathy. Indeed, previous studies verified abnormal expression of microRNA in the retina of OIR mice, which could regulate the formation of neovascularization (Chen et al., 2017b; Rattner et al., 2019). Thus, lncRNAs regulate retinal neovascularization via microRNA.

VEGF plays a pivotal role in retinal neovascularization and, thus, was selected as the fulcrum of our network analysis (Zhou et al., 2019). We found that differentially expressed genes were linked to VEGF expression by analysis of protein interactions and gene function. The claudin family gene claudin-4, which had the highest differential expression in the OIR group, encodes a vital tight junction protein mainly expressed in epithelial cells and endothelial cells. Claudin-4 is highly expressed in breast, prostate, and ovarian cancers, and participates in angiogenesis of ovarian cancer (Li et al., 2009; Rambabu and Jayanthi, 2018). In addition, claudin-4 is highly expressed during neovascularization of the corneal endothelium (Chng et al., 2013), whereas claudin-1, -2, and -5 are highly expressed in OIR tissues of mice, consistent with our experimental results (Luo et al., 2011). However, further studies are needed to determine the specific upstream regulatory mechanism involved and its relationship to lncRNA.

In conclusion, bioinformatics methods can provide a practical approach to screen lncRNAs associated with ROP. However, this study still has significant limitations. First, as it is difficult to obtain clinical tissue samples of ROP, the current experimental studies are based on OIR of mice. Second, the study lacked in-depth analysis of specific genes involved in ROP. As such, more investigations including analyses of larger sample sizes and clinical samples are required to determine the biological functions and regulatory mechanisms of lncRNAs associated with ROP, thus providing a theoretical framework for clinical research and development of new treatments.

Author contributions: *Study design: YD; study implementation: YW, XW; data collection and analysis: YM, YXW; manuscript writing: YW. All authors approved the final version of the paper.*
Conflicts of interest: *The authors declare that they have no competing interests.*
Financial support: *The work was supported by the National Natural Science Foundation of China, No. 81600747 (to YD) and Startup Foundation for Doctors of Liaoning Province, China, No. 201501020 (to YD). The funders had no roles in the study design, conduction of experiment, data collection and analysis, decision to publish, or preparation of the manuscript.*
Institutional review board statement: *This study was approved by the Medical Ethics Committee of Shengjing Hospital of China Medical University on February 25, 2016 (approval No. 2016PS074K). All experimental procedures were performed in accordance with the National Institutes of Health (NIH) guidelines for the Care and Use of Laboratory Animals (NIH Publication No. 85-23, revised 1996).*
Copyright license agreement: *The Copyright License Agreement has been signed by all authors before publication.*
Data sharing statement: *Datasets analyzed during the current study are available from the corresponding author on reasonable request.*
Plagiarism check: *Checked twice by iThenticate.*
Peer review: *Externally peer reviewed.*

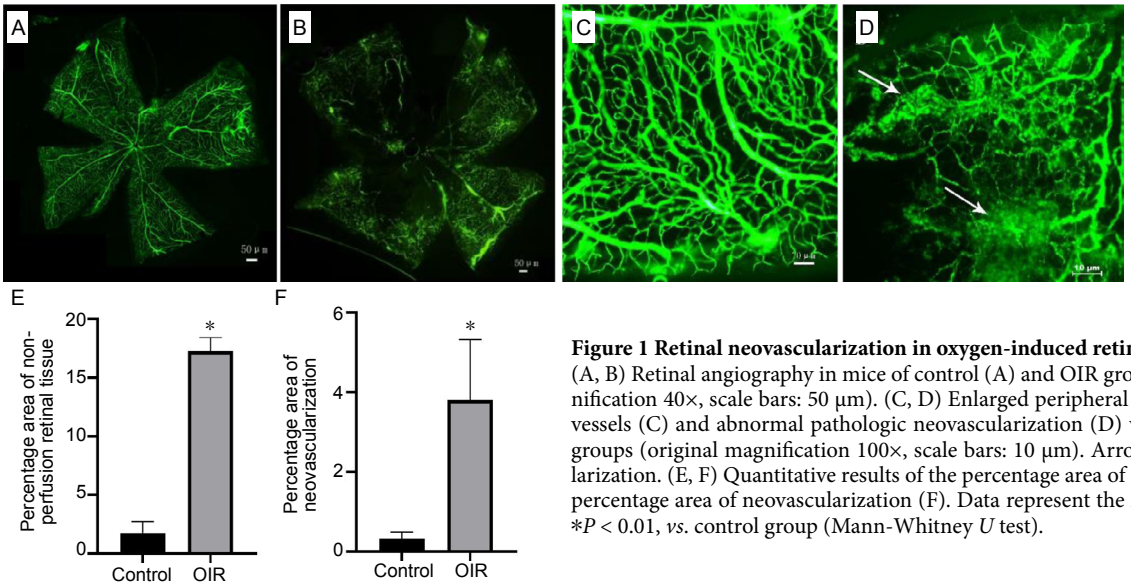

Figure 1 Retinal neovascularization in oxygen-induced retinopathy (OIR) mice.
(A, B) Retinal angiography in mice of control (A) and OIR groups (B) (original magnification 40×, scale bars: 50 μm). (C, D) Enlarged peripheral retina areas of normal vessels (C) and abnormal pathologic neovascularization (D) were observed in both groups (original magnification 100×, scale bars: 10 μm). Arrows indicate neovascularization. (E, F) Quantitative results of the percentage area of non-perfusion (E) and percentage area of neovascularization (F). Data represent the mean ± SEM (n = 15). $*P < 0.01$, *vs.* control group (Mann-Whitney U test).

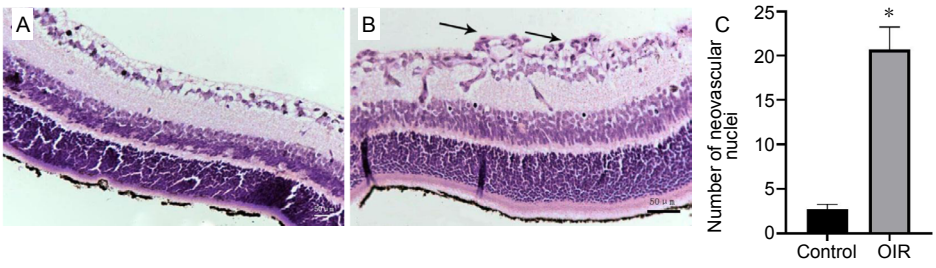

Figure 2 Neovascular nuclei of the retina in oxygen-induced retinopathy (OIR) mice.
(A, B) Hematoxylin-eosin staining of retinal tissue in mice from control (A) and OIR groups (B) (original magnification 200×, scale bars: 50 μm). Arrows indicate retinal neovascular nuclei. (C) Quantitative results for the number of neovascular nuclei. Data represent the mean ± SEM (n = 10). $*P < 0.01$, *vs.* control group (Mann-Whitney U test).

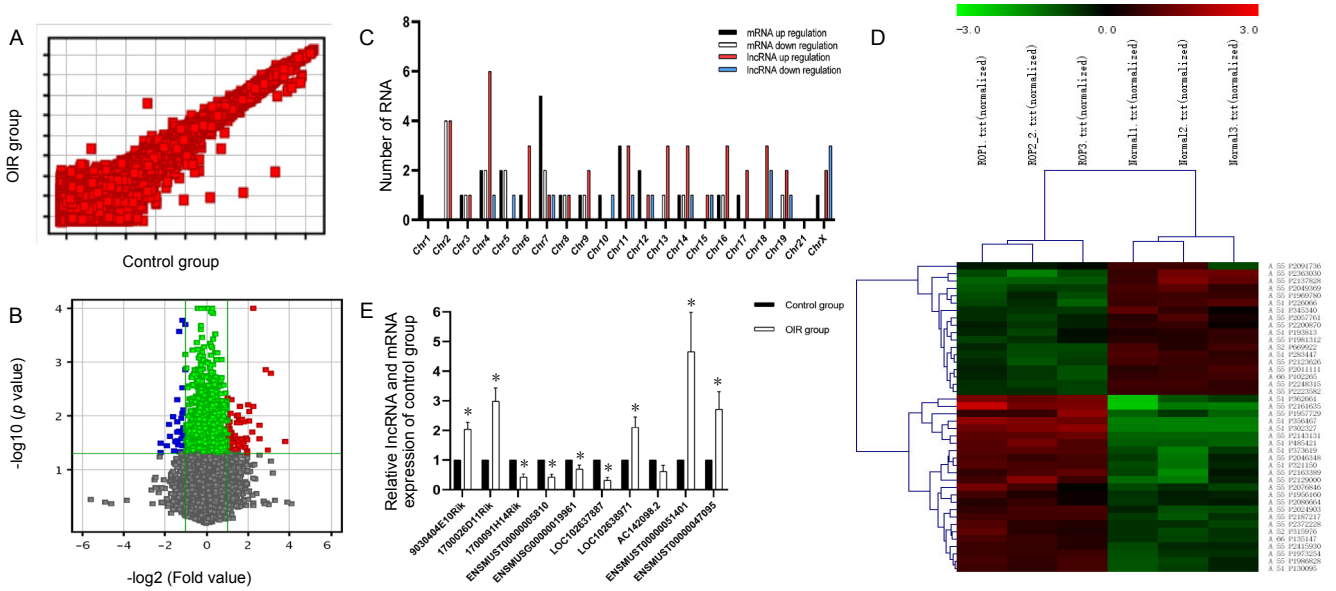

Figure 3 Differentially expressed lncRNAs and mRNAs in the retinal tissue of oxygen-induced retinopathy mice.
(A) Scatter plot of differentially expressed genes. X-axis represents the signal value of this point after standardization in the control chip. Y-axis represents the signal value of this point after standardization in the sample chip. (B) Volcano plot of differentially expressed genes. Gray dots indicate genes with P-values > 0.05. Green dots indicate genes with absolute values of fold change < 2 and P-value ≤ 0.05. Red dots indicate genes with fold change ≥ 2 and P-value ≤ 0.05, which were significantly upregulated differentially expressed genes. Blue dots indicate genes with fold change ≤ –2 and P-value ≤ 0.05, which are significantly downregulated differentially expressed genes. (C) Chromosome distribution of differentially expressed genes. (D) Cluster analysis of differentially expressed genes. Color scale represents the change of gene expression from relatively low (green) to relatively high (red). The line name represents the probe name, while the column name represents the sample name. (E) Validation of differentially expressed genes by real-time polymerase chain reaction. The x-axis represents the gene name, and the Y-axis represents the relative expression of differentially expressed genes. lncRNA: Long noncoding RNA; OIR: oxygen-induced retinopathy.

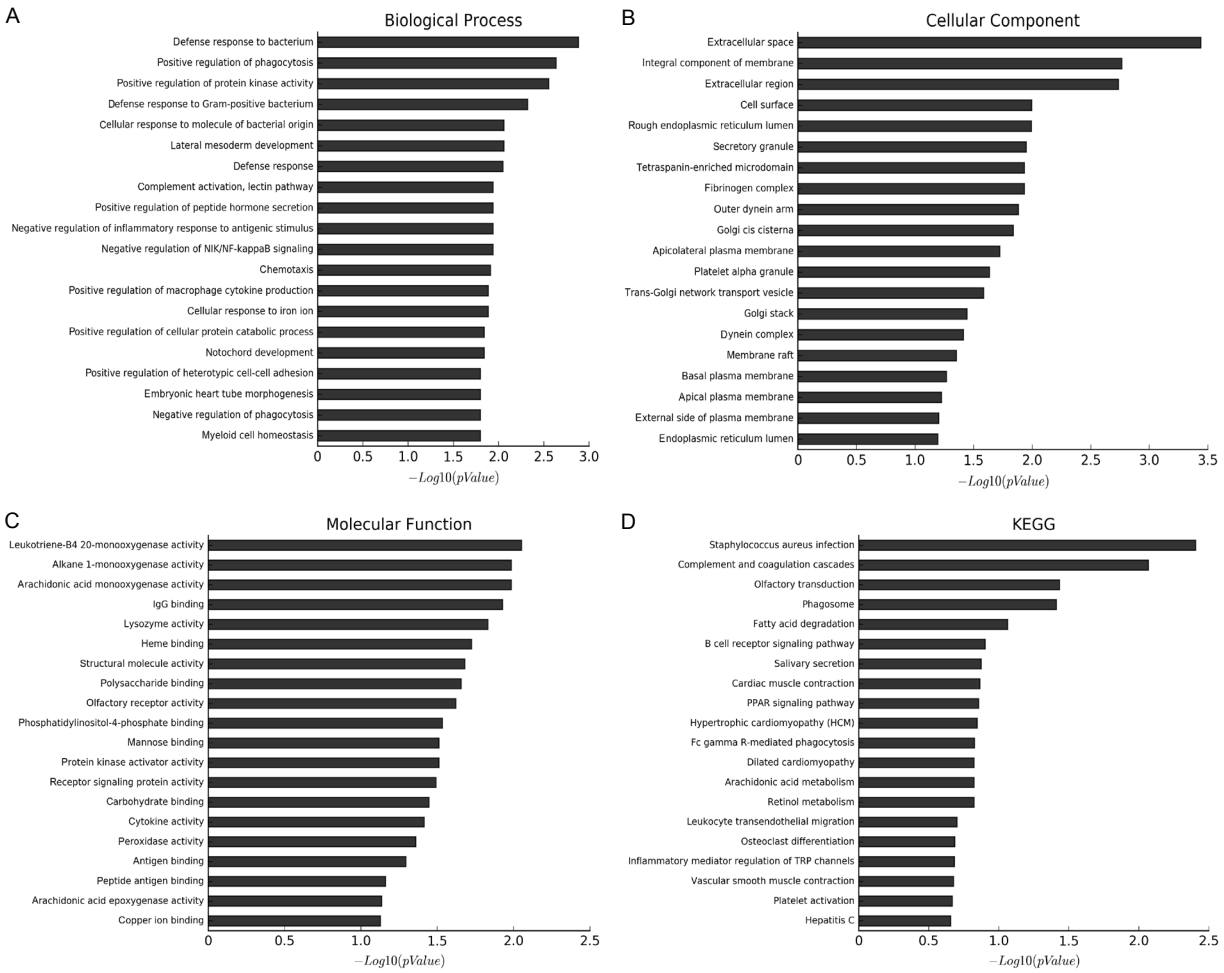

Figure 4 GO analysis and KEGG analysis of differentially expressed genes in the retinal tissue of oxygen-induced retinopathy mice.
(A–C) GO analysis suggests the function of differentially expressed genes, arranged according to *P*-value from small to large. (A) The top 20 biological processes. (B) The top 20 cellular components. (C) The top 20 molecular functions. (D) KEGG analysis: the top 20 pathways. It is suggested that differentially expressed genes may be involved in changes of cellular pathways. GO: Gene Ontology; KEGG: Kyoto Encyclopedia of Genes and Genomes.

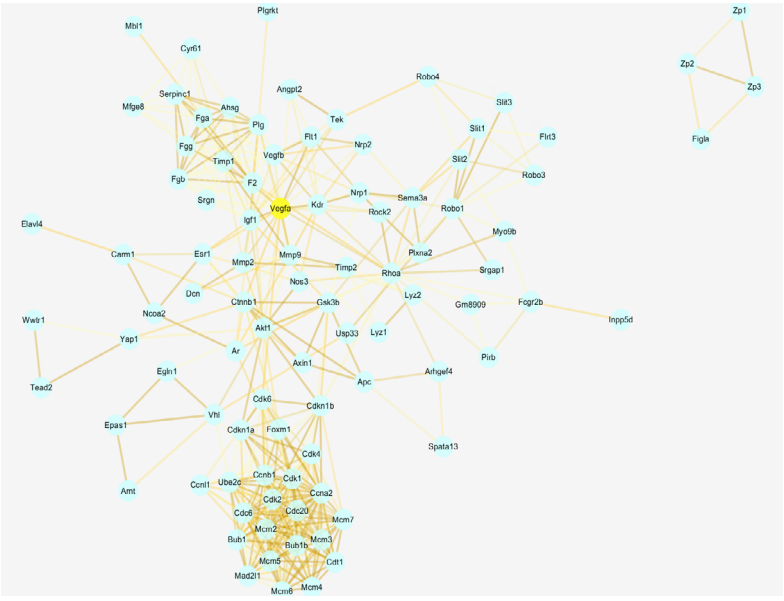

Figure 5 Differentially expressed gene-related protein network of retinal neovascularization.
The yellow area is the center of the network, the blue area represents differentially expressed genes, and the short lines represent interactions between differentially expressed mRNAs; darker lines indicate a stronger interaction. This network suggests an interaction between differentially expressed mRNAs, thus providing the basis for exploring the biological functions of these genes.

References

Aranda JV, Qu J, Valencia GB, Beharry KD (2019) Pharmacologic interventions for the prevention and treatment of retinopathy of prematurity. Semin Perinatol 43:360-366.

Banin E, Dorrell MI, Aguilar E, Ritter MR, Aderman CM, Smith ACH, Friedlander J, Friedlander M (2006) T2-TrpRS inhibits preretinal neovascularization and enhances physiological vascular regrowth in OIR as assessed by a new method of quantification. Invest Ophthalmol Visual Sci 47:2125-2134.

Bucher F, Stahl A, Agostini HT, Martin G (2013) Hyperoxia causes reduced density of retinal astrocytes in the central avascular zone in the mouse model of oxygen-induced retinopathy. Mol Cell Neurosci 56:225-233.

Chen W, Yang S, Zhou Z, Zhao X, Zhong J, Reinach PS, Yan D (2017a) The long noncoding RNA landscape of the mouse eye. Invest Ophthalmol Visual Sci 58:6308-6317.

Chen W, Zhang J, Zhang P, Hu F, Jiang T, Gu J, Chang Q (2019) Role of TLR4-MAP4K4 signaling pathway in models of oxygen-induced retinopathy. FASEB J 33:3451-3464.

Chen XK, Ouyang LJ, Yin ZQ, Xia YY, Chen XR, Shi H, Xiong Y, Pi LH (2017b) Effects of microRNA-29a on retinopathy of prematurity by targeting AGT in a mouse model. Am J Transl Res 9:791-801.

Chng Z, Peh GSL, Herath WB, Cheng TYD, Ang HP, Toh KP, Robson P, Mehta JS, Colman A (2013) High throughput gene expression analysis identifies reliable expression markers of human corneal endothelial cells. PLoS One 8:e67546.

Fan G, Gu Y, Zhang J, Xin Y, Shao J, Giampieri F, Battino M (2019) Transthyretin upregulates long non-coding RNA MEG3 by affecting PABPC1 in diabetic retinopathy. Int J Mol Sci 20:6313.

Geng W, Qin F, Ren J, Xiao S, Wang A (2018) Mini-peptide RPL41 attenuated retinal neovascularization by inducing degradation of ATF4 in oxygen-induced retinopathy mice. Exp Cell Res 369:243-250.

Gonski S, Hupp SR, Cotten CM, Clark RH, Laughon M, Watt K, Hornik CP, Kumar K, Smith PB, Greenberg RG (2019) Risk of development of treated retinopathy of prematurity in very low birth weight infants. J Perinatol 39:1562-1568.

Heiduschka P, Plagemann T, Li L, Alex AF, Eter N (2019) Different effects of various anti-angiogenic treatments in an experimental mouse model of retinopathy of prematurity. Clin Exp Ophthalmol 47:79-87.

Hui Y, Yin Y (2018) MicroRNA-145 attenuates high glucose-induced oxidative stress and inflammation in retinal endothelial cells through regulating TLR4/NF-κB signaling. Life Sci 207:212-218.

Ishikawa M, Sawada Y, Yoshitomi T (2015) Structure and function of the interphotoreceptor matrix surrounding retinal photoreceptor cells. Exp Eye Res 133:3-18.

Kang HG, Choi EY, Byeon SH, Kim SS, Koh HJ, Lee SC, Kim M (2019) Intravitreal ranibizumab versus laser photocoagulation for retinopathy of prematurity: efficacy, anatomical outcomes and safety. Br J Ophthalmol 103:1332-1336.

Le YZ (2017) VEGF production and signaling in Müller glia are critical to modulating vascular function and neuronal integrity in diabetic retinopathy and hypoxic retinal vascular diseases. Vision Res 139:108-114.

Li Calzi S, Shaw LC, Moldovan L, Shelley WC, Qi X, Racette L, Quigley JL, Fortmann SD, Boulton ME, Yoder MC, Grant MB (2019) Progenitor cell combination normalizes retinal vascular development in the oxygen-induced retinopathy (OIR) model. JCI Insight 4:e129224.

Li J, Chigurupati S, Agarwal R, Mughal MR, Mattson MP, Becker KG, Wood WH 3rd, Zhang Y, Morin PJ (2009) Possible angiogenic roles for claudin-4 in ovarian cancer. Cancer Biol Ther 8:1806-1814.

Liu R, Liao X, Li X, Wei H, Liang Q, Zhang Z, Yin M, Zeng X, Liang Z, Hu C (2018) Expression profiles of long noncoding RNAs and mRNAs in post-cardiac arrest rat brains. Mol Med Rep 17:6413-6424.

Long FQ, Su QJ, Zhou JX, Wang DS, Li PX, Zeng CS, Cai Y (2018) LncRNA SNHG12 ameliorates brain microvascular endothelial cell injury by targeting miR-199a. Neural Regen Res 13:1919-1926.

Luo Y, Xiao W, Zhu X, Mao Y, Liu X, Chen X, Huang J, Tang S, Rizzolo LJ (2011) Differential expression of claudins in retinas during normal development and the angiogenesis of oxygen-induced retinopathy. Invest Ophthalmol Visual Sci 52:7556-7564.

Ma QQ, Liu FY, Shi M, Sun CH, Tan Z, Chang XD, Li QP, Feng ZC (2019) Bone marrow mesenchymal stem cells modified by angiogenin-1 promotes tissue repair in mice with oxygen-induced retinopathy of prematurity by promoting retinal stem cell proliferation and differentiation. J Cell Physiol 234:21027-21038.

Mehdi MK-IM, Sage-Ciocca D, Challet E, Malan A, Hicks D (2014) Oxygen-induced retinopathy induces short-term glial stress and long-term impairment of photoentrainment in mice. Graefes Arch Clin Exp Ophthalmol 252:595-608.

Morken TS, Dammann O, Skranes J, Austeng D (2019) Retinopathy of prematurity, visual and neurodevelopmental outcome, and imaging of the central nervous system. Semin Perinatol 43:381-389.

Nieminen T, Scott TA, Lin FM, Chen Z, Yla-Herttuala S, Morris KV (2018) Long non-coding RNA modulation of VEGF-A during hypoxia. Noncoding RNA 4:34.

Park K, Chen Y, Hu Y, Mayo AS, Kompella UB, Longeras R, Ma JX (2009) Nanoparticle-mediated expression of an angiogenic inhibitor ameliorates ischemia-induced retinal neovascularization and diabetes-induced retinal vascular leakage. Diabetes 58:1902-1913.

Qiu GZ, Tian W, Fu HT, Li CP, Liu B (2016) Long noncoding RNA-MEG3 is involved in diabetes mellitus-related microvascular dysfunction. Biochem Biophys Res Commun 471:135-141.

Qu G, Shi H, Wang B, Li S, Zhang A, Gan W (2017) Alterations in the long non-coding RNA transcriptome in mesangial cells treated with aldosterone in vitro. Mol Med Rep 16:6004-6012.

Rambabu M, Jayanthi S (2018) Virtual screening of National Cancer Institute database for claudin-4 inhibitors: Synthesis, biological evaluation, and molecular dynamics studies. J Cell Biochem doi:10.1002/jcb.28147.

Rattner A, Williams J, Nathans J (2019) Roles of HIFs and VEGF in angiogenesis in the retina and brain. J Clin Invest 130:3807-3820.

Ruan W, Zhao F, Zhao S, Zhang L, Shi L, Pang T (2018) Knockdown of long noncoding RNA MEG3 impairs VEGF-stimulated endothelial sprouting angiogenesis via modulating VEGFR2 expression in human umbilical vein endothelial cells. Gene 649:32-39.

Shen Y, Dong LF, Zhou RM, Yao J, Song YC, Yang H, Jiang Q, Yan B (2016) Role of long non-coding RNA MIAT in proliferation, apoptosis and migration of lens epithelial cells: a clinical and in vitro study. J Cell Mol Med 20:537-548.

Shi S, Li X, Li Y, Pei C, Yang H, Chen X (2013) Expression and function of Delta-like ligand 4 in a rat model of retinopathy of prematurity. Neural Regen Res 8:723-730.

Smith LE, Wesolowski E, McLellan A, Kostyk SK, D'Amato R, Sullivan R, D'Amore PA (1994) Oxygen-induced retinopathy in the mouse. Invest Ophthalmol Visual Sci 35:101-111.

Troullinaki M, Alexaki VI, Mitroulis I, Witt A, Klotzsche-von Ameln A, Chung KJ, Chavakis T, Economopoulou M (2019) Nerve growth factor regulates endothelial cell survival and pathological retinal angiogenesis. J Cell Mol Med 23:2362-2371.

Tsang JKW, Liu J, Lo ACY (2019) Vascular and neuronal protection in the developing retina: potential therapeutic targets for retinopathy of prematurity. Int J Mol Sci 20:4321.

Wang H, Liao S, Li H, Chen Y, Yu J (2019) Long non-coding RNA TUG1 sponges mir-145a-5p to regulate microglial polarization after oxygen-glucose deprivation. Front Mol Neurosci 12:215.

Wang S, Sorenson CM, Sheibani N (2005) Attenuation of retinal vascular development and neovascularization during oxygen-induced ischemic retinopathy in Bcl-2$^{-/-}$ mice. Dev Biol 279:205-219.

Wei JC, Shi YL, Wang Q (2019) LncRNA ANRIL knockdown ameliorates retinopathy in diabetic rats by inhibiting the NF-κB pathway. Eur Rev Med Pharmacol Sci 23:7732-7739.

Xu W, Hu Z, Lv Y, Dou G, Zhang Z, Wang H, Wang Y (2018) Microglial density determines the appearance of pathological neovascular tufts in oxygen-induced retinopathy. Cell Tissue Res 374:25-38.

Xu XD, Li KR, Li XM, Yao J, Qin J, Yan B (2014) Long non-coding RNAs: new players in ocular neovascularization. Mol Biol Rep 41:4493-4505.

Yang LX, Yang LK, Zhu J, Chen JH, Wang YH, Xiong K (2019) Expression signatures of long non-coding RNA and mRNA in human traumatic brain injury. Neural Regen Res 14:632-641.

Yao J, Shi Z, Ma X, Xu D, Ming G (2019) lncRNA GAS5/miR-223/NAMPT axis modulates the cell proliferation and senescence of endothelial progenitor cells through PI3K/AKT signaling. J Cell Biochem 120:14518-14530.

You D, You H (2019) Repression of long non-coding RNA MEG3 restores nerve growth and alleviates neurological impairment after cerebral ischemia-reperfusion injury in a rat model. Biomed Pharmacother 111:1447-1457.

Young TL, Matsuda T, Cepko CL (2005) The noncoding RNA taurine upregulated gene 1 is required for differentiation of the murine retina. Curr Biol 15:501-512.

Yu L, Fu J, Yu N, Wu Y, Han N (2019) Long non-coding RNA MALAT1 participates in the pathological angiogenesis of diabetic retinopathy in oxygen-induced retinopathy mouse model by sponging miR-203a-3p. Can J Physiol Pharmacol doi:10.1139/cjpp-2019-0489.

Zhang C, Qu Y, Xiao H, Xiao W, Liu J, Gao Y, Li M, Liu J (2019a) LncRNA SNHG3 promotes clear cell renal cell carcinoma proliferation and migration by upregulating TOP2A. Exp Cell Res 384:111595.

Zhang LQ, Cui H, Wang L, Fang X, Su S (2017) Role of microRNA-29a in the development of diabetic retinopathy by targeting AGT gene in a rat model. Exp Mol Pathol 102:296-302.

Zhang L, Dong Y, Wang Y, Gao J, Lv J, Sun J, Li M, Wang M, Zhao Z, Wang J, Xu W (2019b) Long non-coding RNAs in ocular diseases: new and potential therapeutic targets. FEBS J 286:2261-2272.

Zhang S, Leske DA, Holmes JM (2000) Neovascularization grading methods in a rat model of retinopathy of prematurity. Invest Ophthalmol Visual Sci 41:887-891.

Zhang X, Zhu XL, Ji BY, Cao X, Yu LJ, Zhang Y, Bao XY, Xu Y, Jin JL (2019c) LncRNA-1810034E14Rik reduces microglia activation in experimental ischemic stroke. J Neuroinflammation 16:75-75.

Zhou TE, Zhu T, Rivera JC, Omri S, Tahiri H, Lahaie I, Rouget R, Wirth M, Nattel S, Lodygensky G, Ferbeyre G, Nezhady M, Desjarlais M, Hamel P, Chemtob S (2019) The inability of the choroid to revascularize in oxygen-induced retinopathy results from increased p53/miR-Let-7b activity. Am J Pathol 189:2340-2356.

Zhu D, Fang C, Li X, Geng Y, Li R, Wu C, Jiang J, Wu C (2017) Predictive analysis of long non-coding RNA expression profiles in diffuse large B-cell lymphoma. Oncotarget 8:23228-23236.

C-Editor: Zhao M; S-Editors: Yu J, Li CH; L-Editors: Van Deusen A, Yu J, Song LP; T-Editor: Jia Y